

AOSLO: from Benchtop to Clinic

Yuhua Zhang, Siddharth Poonja, Austin Roorda
School of Optometry, University of California, Berkeley, CA 94720

ABSTRACT

We present a clinically deployable adaptive optics scanning laser ophthalmoscope (AOSLO) that features micro-electro-mechanical (MEMS) deformable mirror (DM) based adaptive optics (AO) and low coherent light sources. With the miniaturized optical aperture of a μ DMS-Multi™ MEMS DM (Boston Micromachines Corporation, Watertown, MA), we were able to develop a compact and robust AOSLO optical system that occupies a 50 cm X 50 cm area on a mobile optical table. We introduced low coherent light sources, which are superluminescent laser diodes (SLD) at 680 nm with 9 nm bandwidth and 840 nm with 50 nm bandwidth, in confocal scanning ophthalmoscopy to eliminate interference artifacts in the images. We selected a photo multiplier tube (PMT) for photon signal detection and designed low noise video signal conditioning circuits. We employed an acoustic-optical (AOM) spatial light modulator to modulate the light beam so that we could avoid unnecessary exposure to the retina or project a specific stimulus pattern onto the retina. The MEMS DM based AO system demonstrated robust performance. The use of low coherent light sources effectively mitigated the interference artifacts in the images and yielded high-fidelity retinal images of contiguous cone mosaic. We imaged patients with inherited retinal degenerations including cone-rod dystrophy (CRD) and retinitis pigmentosa (RP). We have produced high-fidelity, real-time, microscopic views of the living human retina for healthy and diseased eyes.

Key words: scanning laser ophthalmoscope; adaptive optics; MEMS; deformable mirror; detection; retina

1. INTRODUCTION

The first adaptive optics scanning laser ophthalmoscope (AOSLO) reported by Roorda et al.¹ has been demonstrated to produce microscopic views of the living human retina with unprecedented optical quality. It yielded the first real-time images of photoreceptors and blood flow in living human retina at video rates. The synergetic incorporation of scanning laser ophthalmoscopy^{2, 3} (SLO) with adaptive optics (AO) is the most critical feature of AOSLO. The merits of confocal imaging such as enhanced resolution and fine optical sectioning ability have been well treated by Webb et al.^{3, 4}, Roorda⁵, Sheppard and Shotten⁶ and Wilson and Sheppard⁷. The use of AO to correct the ocular aberrations⁸⁻¹⁰ of the human eye (which is the objective lens of SLO) bestows the confocal SLO with all the fundamental merits of a confocal scanning imaging mechanism, and thus empowers us to image the human retina *in vivo* at microscopic rather than macroscopic spatial scale¹¹⁻¹³. This capability greatly facilitates efforts to reveal retinal disease mechanisms¹⁴⁻¹⁶ and improve diagnosis¹⁷. AOSLO has become an attractive microscopic imaging modality for living human eyes.

The first AOSLO was a lab-deployed system. It employed a 37-channel mechanical DM (Xinetics Inc., Devens, MA), which is a continuous mirror face sheet offering a 46mm effective optical aperture that is fixed to an array of individually addressable, discrete piezoelectric actuators. In order to map the human pupil to the effective aperture of the DM, relay telescopes with large magnification ratios had to be applied thus leading to a fairly large overall system structure which occupied about 1.5 m×1 m area on an optical table¹. For clinic applications, it is highly desirable that the AOSLO should be robust in performance, compact in structure, and ergonomic in its design.

In this paper, we developed a new generation AOSLO, which aimed at better compensation for the wave aberrations of the eye thereby rendering higher-quality microscopic views of the living retina, all housed in a compact structure that is clinically deployable. To attain these goals, we systematically studied the technical issues including the compact optical system design with the cutting-edge MEMS DM based AO, new light source, optimized photon detection and video signal conditioning circuits.

2. METHODS

2.1. AOSLO General System

Shown in Fig.1 is the general system construction of the new generation AOSLO, which is implemented from a basic configuration that has been described elsewhere¹⁸⁻²⁰. It is equipped with two low coherence light sources which are superluminescent laser diodes (SLD) (Superlum Ltd, Russia) with single mode fiber output. The two SLDs' center wavelengths are 680 nm and 840 nm respectively. The light from the two sources are first collimated (by lenses L1, L4) and relayed (by telescopes L2, L3 and L5, L6) to a dichroic mirror (DC) which reflects the light of the 680 nm SLD but let the light of the 840 nm pass through to the beam splitter (BS) to the DM, the horizontal and vertical scanners (HS, an VS), and finally to the eye, forming a raster scan on the retina. The diffusely reflected light from the retina transmits inversely along the ingoing path to the beam splitter, where most of the light passes through and is relayed by a telescope (L7, L8) to the collection lens L9. A confocal pinhole PH1 is placed at the focal point of the collection lens L9, and the signal is received by the photodetector which is a photomultiplier tube (PMT), further processed by the signal conditioning module SC, and acquired by the computer for storage and display. An avalanche photo diode (APD) detector is in reserve for the 840 nm SLD to achieve better photon detection. In this case the flip mirror FM will bend the light to the APD via pinhole PH2.

An acoustic-optical modulator (AOM) is placed in the 680 nm light path to modulate the beam such that the retina is only illuminated when the imaging acquisition is being conducted. Moreover, by modulating the phase and intensity of the beam, we can generate specific stimulus patterns on the retina²¹.

The optical system occupies about 0.5 m × 0.5 m area on a mobile optical work table while keeping the system aberrations diffraction-limited over an imaging field up to 3 × 3 degrees. Although two computers are employed in this

system, one for adaptive optics and AOM control, and the other for image acquisition, they are both run from a single user interface.

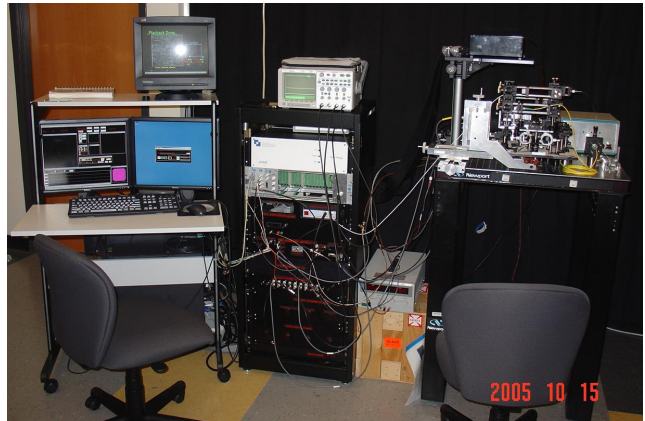
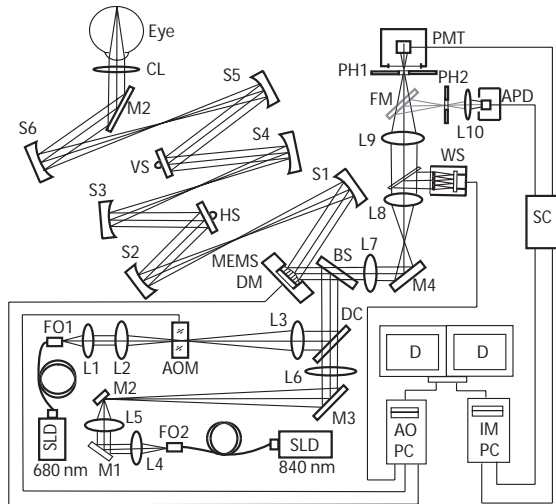


Fig.1. SLD, superluminescent laser diode; FO1, FO2, fiber output; AOPC, computer for AO; IMPC, computer for image acquisition; D, display; BS, beam splitter; HS, horizontal scanner (16KHz); VS, vertical scanner (30, 60 Hz); CL, cylindrical lens; WS, wavefront sensor; PH1, PH2, confocal pinhole; PMT, photomultiplier tube; APD, avalanche photo diode; M1~M4, flat mirrors; S1~S6, spherical mirrors; L1~L10, achromatic lenses; DC, dichroic mirror; SC, signal conditioning module;

2.2. Imaging Protocol

Approvals for image human subjects were obtained by the University of California, Berkeley and the University of California, San Francisco IRBs, and informed consent was obtained from each subject prior to imaging.

In order to attain high resolution imaging, the AOSLO works with a large size pupil. The subjects' eyes were dilated with one topically applied drop each of 0.5 % tropicamide and 2.5 % phenylephrine. The AO correction was done over a 6mm pupil.

The illumination power is governed by the maximum permissible exposure (MPE) levels to the human eye which are regulated by the American Standards for the Safe Use of Lasers (ANSI Z136.1-2000)²². The MPE values are specified by the light wavelength, the eye condition and the scanning field as well as the exposure time. The new generation AOSLO will equip two laser sources whose center wavelengths are 680 nm and 840 nm, respectively. The frame rate is 30 Hz. The subject's eye will be dilated during imaging and the beam size projecting on the cornea is 6mm, which covers an area of 0.283 cm². The scanning field can be as small as 1⁰×1⁰ which covers about 300 × 300 μm² area on the retina. We assume 2 hours exposure time for each imaging session. In addition to the ANSI MPE level, we must ensure that the illumination should not cause severe discomfort for the subjects. So, we take a more conservative approach that adopts a level that will be at least 10 times less than the ANSI MPE. In practice, when the 655 nm diode laser is used, the illumination power at the cornea is 60 μw, which is about 1/50th of what the ANSI

standard considers to be a safe exposure level. Whereas for the 840nm SLD, the illumination power is 300 μ w, which is about 1/37th of what the ANSI standard considers to be a safe exposure level.

Patients used a dental impression mount affixed to an X-Y-Z translation stage to set and maintain eye alignment during the imaging. The retinal location of wavefront correction and imaging was controlled by having the subject view a fixation target. A device which will release the subjects from biting the bite-bar would thus improve the comfort of the subject being tested and hopefully will be incorporated into the system soon.

2.3. MEMS DM based AO

The MEMS DM based AO represents the most important technology advance of the new AOSLO¹⁸⁻²⁰. The MEMS DM is the μ DMS-Multi™ made by Boston Micromachines Corporation (Watertown, MA), which consists of a single membrane supported by an underlying actuator array. Deflection of the mirror surface is via electrostatic attraction, and each actuator is individually addressable. Although this DM has a continuous membrane reflecting surface, it differs from a conventional membrane design. Cross-talk between actuators is minimized by constructing the actuator array with a double cantilever design. The mirror is described in detail elsewhere²³⁻²⁵. The specific mirror array is a 140 actuator design (12 \times 12 with no corner actuators) over a 4.4 mm clear aperture. The actuator stroke is 3.5 microns. It just meets the AO the requirements on the wavefront corrector for compensation of high order aberrations in the human eyes²⁵⁻²⁸. A Shack-Hartmann wavefront sensor was built to facilitate the AO system. The lenslet array has a 0.328 mm \times 0.328 mm pitch with a 24 mm focal length. The DM, the lenslet array of the Shack-Hartmann wavefront sensor, the HS, VS and the collection lens are aligned such that they are all conjugate to the entrance pupil of the eye. The wavefront is corrected for both the ingoing path (for a sharp focus on the retina) and the outgoing path (for a sharp image of the focused spot on the confocal pinhole). A modal approach is adopted to run the AO closed loop. A 10th order Zernike polynomial is fitted to the wavefront slopes. The actuator deflections are then calculated directly from the best fit wavefront. We adopted a proportional control strategy and achieved a closed-loop update frequency about 10 Hz.

2.4. Low Coherent Light Sources

The introduction of low coherent light sources in AOSLO is another feature of the new instrument^{18, 29, 30}. As shown in Fig.2, the image taken with the SLD shows the contiguous cone mosaic more clearly while the image taken with the laser diode, because of interference, has spuriously high contrast. Evidently, the low coherent light source renders a higher fidelity image of the retina.

The 680 nm red SLD has a 9 nm spectrum FWHM and the 840 nm infra-red SLD has a 50 nm spectrum FWHM (Broadlighter S840-HP, Superlum, Russia). The infra-red SLD, compared with the visible red one, which has deeper penetration in the retina and is more comfortable and less hazardous, is used for patient imaging, while the

visible red SLD is designated for sending a stimulus to the retina for microperimetry, testing retinal function, and performing visual psychophysics research.

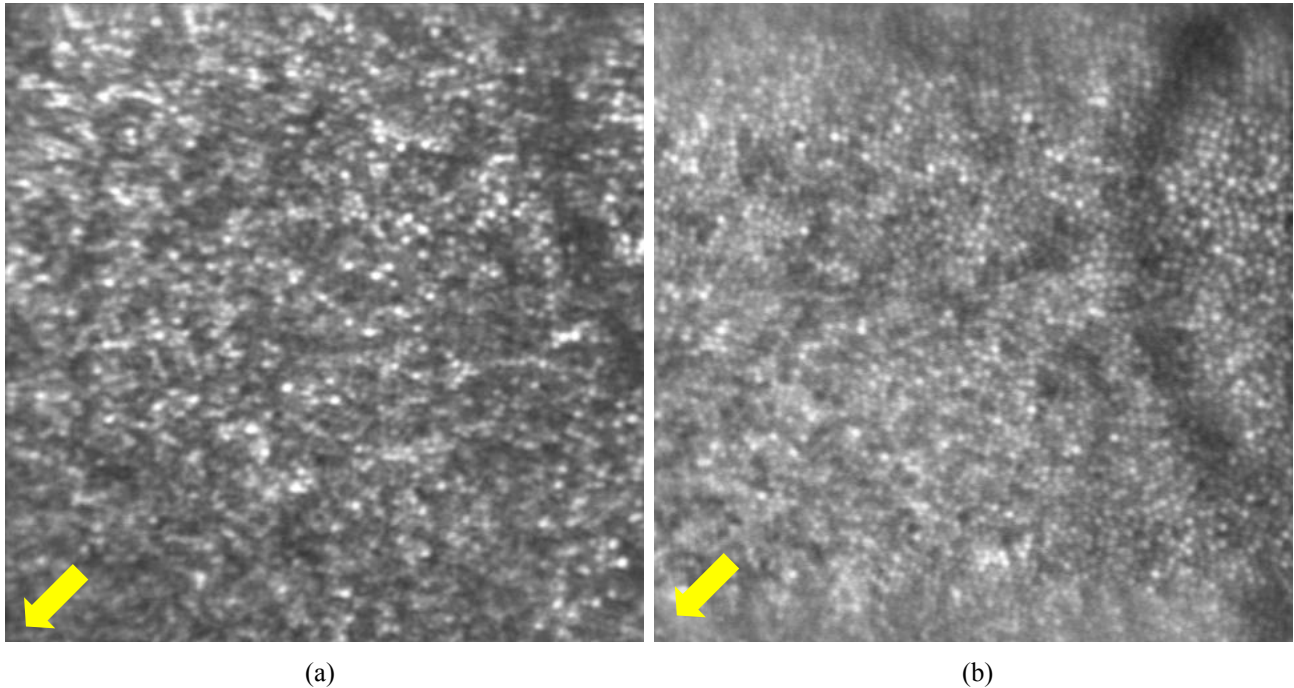


Fig.2. (a) is registered image from a set of 10 AO-corrected frames. The image was taken with the 840nm diode laser. Whereas (b) is a registered image which was taken with the 840nm SLD. All images have been corrected for distortions due to eye movements³². These images were taken from a retinal location about 0.6 degree from the center of the fovea. The arrows point in the direction of the foveal center. The field of view subtends 1.2 degrees, or approximately 360 μm on a side. All the images were taken with the same illumination power level and the same settings of the AOSLO imaging system.

2.5. Photon Signal Detection

A properly selected photo-detector which gives good signal to noise ratio (SNR) is of particular significance in achieving the full potential of the AOSLO. SNR is an important criterion for choosing a suitable detector from the selection of photomultiplier tubes (PMT) and avalanche photodiodes (APD), which are two types of commercially available photo-detectors that may technically be used in the development of the new AOSLO. We selected 4 PMTs and 3 APDs which matched the light source spectral characteristics and had good quantum efficiency and calculated the SNR of each photo-detector. We also considered other factors such as maximum exposure power level (detector operation range), easy of use with least effort on manufacturing the complicated but necessary transimpedance amplifier. Finally, a PMT H7422-20 (Hamamatsu Co., Japan) was chosen for the new AOSLO. The real performance of the selected detector demonstrated good consistency with the theoretical expectations and was further proved in AOSLO imaging applications. Fig.3 shows the calibrated SNR vs. the theoretical analysis.

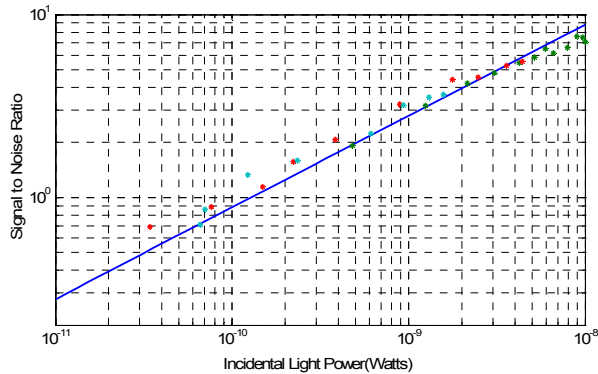


Fig.3, Measured SNR (stars) vs. theoretical calculation (line). PMT H7422-20 over a bandwidth of 10MHz. Light wavelength is 840 nm.

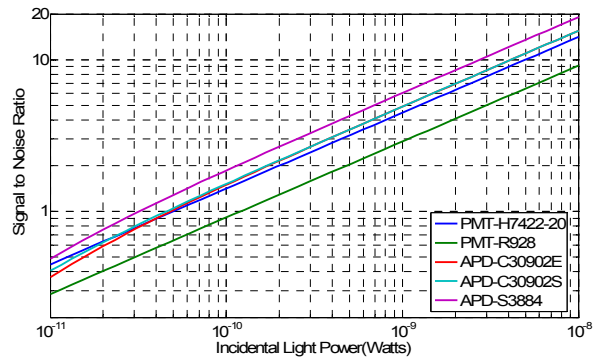


Fig.4 The SNR of 5 photo-detectors with an ideal transimpedance amplifier over a bandwidth of 10MHz. Light wavelength is 680 nm.

PMT is not the only detector that is suitable for AOSLO imaging. The selection was made under the condition that we adopted a commercially available transimpedance amplifier which has fairly high input noise current density. Fig.4 plots the SNR of 5 detectors assuming an ideal transimpedance amplifier whose input noise power spectrum is 0 over the AOSLO signal power range. The theoretical analysis proved that APD model # C30902S (Perkin Elmer Inc., Canada) would give a comparable SNR to that of the PMT H7422-20 once the input noise current density of the transimpedance amplifier was less than $5\text{pA/Hz}^{1/2}$. As for the APD #S3884 (Harmamatsu Co., Japan), because the internal gain is only 50, its requirements on the amplifier are even harsher.

2.6. Imaging Signal Conditioning and Acquisition

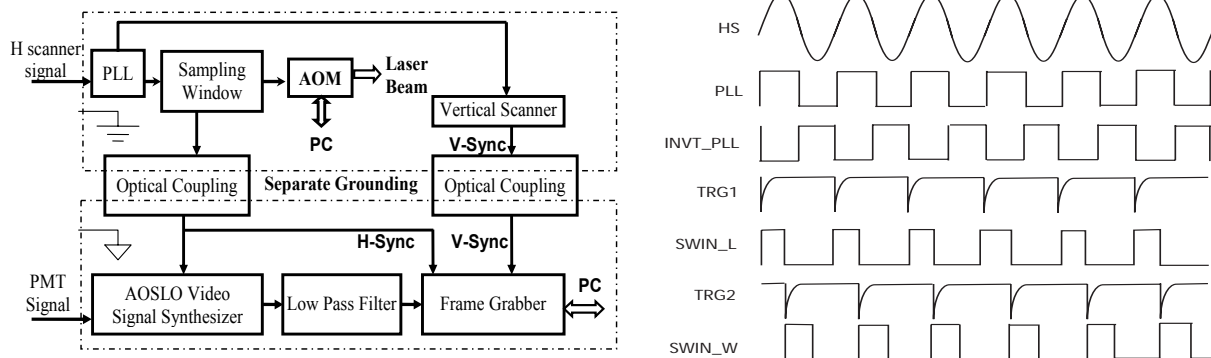


Fig.5. AOSLO imaging signal conditioning and timing

A frame grabber (Helios-XA, Matrox, Montreal, Canada) was adopted to digitize the analog voltage signal coming from the photodetector and generate 8-bit 512×512 frames at 30 frames per second. The signal was conditioned to a pseudo-video format that included black level and active line signals before it was fed into the frame grabber, while

the horizontal (line) and vertical (frame) synchronization signals were fed into the frame grabber separately. Images were acquired and stored uncompressed in a digital format.

As depicted in Fig.5, a phase locked-loop (PLL) is designed to produce a square wave that is in phase with the sinusoidal line scanning signal, which is the master clock of the imaging system. A trigger signal TRG1 is derived from the falling edge of the inverted PLL output. With a proper delay from TRG1, a second trigger signal TRG2 is generated as the starting edge of the sampling window. A sampling window corresponding to the most linear part of the sinusoidal scanning path of the horizontal scanner, which is about 40% of one cycle of the horizontal scan, is formed and sent to the AOM controller to modulate the laser beam such that the light is only projected on the retina within the sampling window and during the rest of cycle there is no light on the retina. Within this window, the computer can also send a more sophisticated control signal to the AOM for phase and intensity modulation of the beam²¹. The sampling window signal is sent to the video signal synthesizer via an optical coupler. The PLL signal is also sent to the vertical scanner driver which gives the vertical (frame) synchronization signal. V-Sync is sent to the frame grabber via an optical coupler. Separate grounding design is adopted to prevent the pseudo-video signal from being affected by the noisy PLL circuit and the AOM as well as the vertical scanner driver modules.

2.7. Light Beam Modulation

Within the sampling window, the computer can also send a more sophisticated control signal to the AOM to modulate both phase and intensity of the beam thus producing a specific stimulus pattern²¹. This function is very useful for microperimetry, or for psychophysics research. In Fig.6, the photo is mapped to the scanning field and decomposed into line digital signal in accordance with the AOSLO imaging system timing. The grey level of each point of the photo is converted to voltage for modulation of the beam intensity at the exact corresponding point of the scanning field. Thus, the scanning beam projects the photo on the retina. With AO correction for ocular aberration, the subject sees a very clear photo. This image is a single frame of a 1.2^o field of view, 512 X 512 pixels video taken at 30 frames per second.

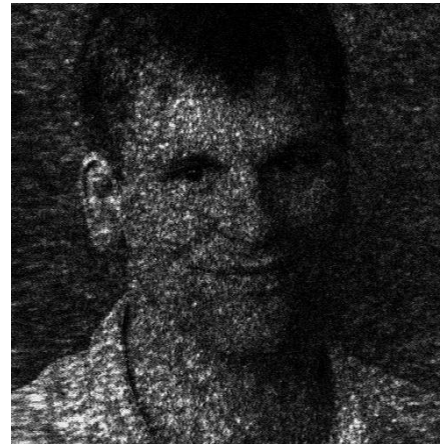


Fig.6. AOSLO projects a photo on the retina by modulating laser beam

3. RESULTS

To date, we have imaged nearly 40 human subjects including 17 retinal degeneration patients. In most cases, the AO reduced the root mean square wave aberration over a 6 mm pupil from 0.4 μ m to less than 0.1 μ m. The robustness of the MEMS DM based AO is also demonstrated by its formation of a very compact focused spot at the confocal pinhole via the collection lens. This enables us to use smaller pinholes while maintaining a decent signal to noise ratio for imaging, and thus bestows better axial resolution³¹. The AO correction, consequently, demonstrates a

threefold benefit for imaging which includes: increased brightness, improved contrast and enhanced resolution of the images.

The new AOSLO has produced high quality retinal images in healthy eyes¹⁸⁻²⁰. Fig.7 further proves that the new AOSLO can achieve the same performance in the eyes of aged subjects.

AOSLO has been used to render high resolution microscopic images of diseased eyes and has revealed microstructures of retinal diseases which are invisible with conventional retinal imaging modalities. For example we recently reported significant increases in cone spacing near the fovea in patients with early stage cone-rod dystrophy, despite the fact that they could see with 20/20 acuity. Conversely, most patients with retinitis pigmentosa had normal cone spacing near the fovea, even in relatively advanced cases^{30, 33}. Furthermore, we have shown, for the first time, direct images of RPE cells in cone-rod dystrophy patients, purportedly in regions where the cones have atrophied (paper in preparation).

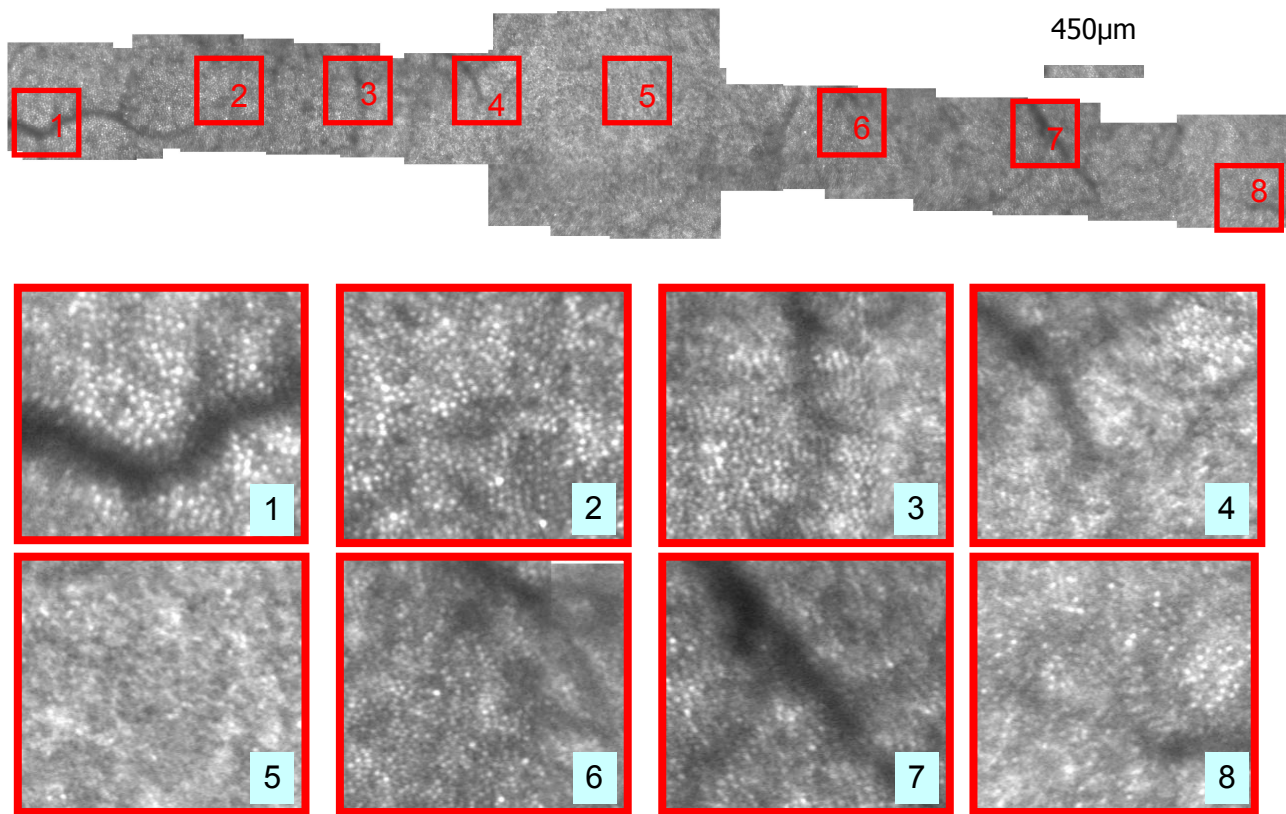


Fig.7, The top image is a composite made by stitching together a series of frames from nasal to temporal spanning about 16 degrees. The middle and bottom images are enlarged views of the retinal areas indicated by the squares in the top image. Except for the very central field, i.e. square 5, the images show a well resolved and contiguous cone mosaic. These images also show photoreceptors ranging in size as a function of eccentricity from the fovea. The scale bar spans 1.5 degrees visual angle. The images were taken with the 840nm SLD light source. All images have been corrected for distortions due to eye movements³². The subject was 58 years old.

4. CONCLUSION

We have developed a new generation AOSLO which features a MEMS DM and low coherence light sources. We have produced high-fidelity, real-time, microscopic views of the living human retina with the new instrument. The new AOSLO has been demonstrated to work effectively for both healthy (40 subjects) and diseased eyes (17 patients) over an age span from 19 to 69 years old. It has revealed microstructures of retinal diseases which are invisible with conventional retinal imaging modalities.

ACKNOWLEDGEMENTS

This work is funded by the NIH Bioengineering Research Partnership grant EY014365 and the National Science Foundation Science and Technology Center for Adaptive Optics, managed by the University of California, Santa Cruz under cooperative agreement #AST-9876783.

REFERENCES:

1. A. Roorda, F. Romero-Borja, W. J. Donnelly, H. Queener, T. J. Hebert and M. C. W. Campbell, "Adaptive optics scanning laser ophthalmoscopy", *Optics Express* **10**, 405-412, 2002.
2. R. H. Webb and G. W. Hughes, "Scanning laser ophthalmoscope", *IEEE Trans. Biomed. Eng.*, **28**, 488-492, 1981.
3. R. H. Webb, G. W. Hughes, and F. C. Delori, "Confocal scanning laser ophthalmoscope", *Appl.Opt.*, **26**, 492-1499, 1987.
4. R.H. Webb, "Confocal optical microscopy", *Reports on Progress in Physics*, **59**, 427 – 451, 1996.
5. A. Roorda, Double Pass Reflections in the Human Eye, Ph.D. thesis, University of Waterloo, Waterloo, Ontario, Canada, 1996.
6. C.J.R. Sheppard and D.M. Shotton, *Confocal microscopy*, Springer-Verlag New York Inc., New York, 1997.
7. T. Wilson and C. J. R. Sheppard, *Theory and Practice of Scanning Optical Microscopy*, Academic Press, London, 1984.
8. J. Liang, D. R. Williams, and D. T. Miller, "Supernormal vision and high-resolution retinal imaging through adaptive optics", *J. Opt. Soc. Am. A*, **14**, 2884-2892, 1997.
9. D.R. Williams, J. Liang, D.T. Miller, and A. Roorda, "Wavefront Sensing and Compensation for the Human Eye", Chap.10 in *Adaptive Optics Engineering Handbook*, R. K. Tyson, Eds., pp.287-310, Marcel Dekker, New York, 2000.
10. A. Roorda and D. R. Williams, "The arrangement of the three cone classes in the living human eye", *Nature*, **397**, 520-522, 1999.
11. K. Venkateswaran, F. Romero-Borja and A. Roorda. "Theoretical Modeling and Evaluation of the Axial Resolution of the Adaptive Optics Scanning Laser Ophthalmoscope," *J. Biomed. Opt.* **9**, 132-138, 2004.
12. Y. Zhang, A. Roorda, "Evaluating the Lateral Resolution of the Adaptive Optics Scanning Laser Ophthalmoscope." *J. Biomed. Opt.* **11**, 014002, 2006.

13. F. Romero-Borja, K. Venkateswaran, A. Roorda, and T.J. Hebert, "Optical Slicing of Human Retinal Tissue in vivo with the Adaptive Optics Scanning Laser Ophthalmoscope," *Appl. Opt.* **44**, 4032-4040, 2005.
14. J.A. Martin and A. Roorda, "Direct and non-Invasive assessment of parafoveal capillary leukocyte velocity", *Ophthalmology*, **112**, 2219-2224, 2005.
15. A. S. Vilupuru, N.V. Rangaswamy, L.J. Frishman, R.S. Harwerth, and A. Roorda, "Adaptive optics ophthalmoscopy for imaging of the lamina cribrosa in glaucoma," *Invest. Ophthalmol. Vis. Sci.*, **46**, E-Abstract, 3515, 2005.
16. J. Carroll, M. Neitz, H. Hofer, J. Neitz, and D. R. Williams. "Functional photoreceptor loss revealed with adaptive optics: an alternate cause of color blindness", *Proc. Natl. Acad. Sci. U.S.A* , **101**, 8461-8466, 2004.
17. J. I. Wolfing, M. Chung, J. Carroll, A. Roorda, and D.R. Williams, "High resolution imaging of cone-rod dystrophy," *Ophthalmol.*, **113**, 1014-1019, 2006.
18. Y. Zhang, S. Poonja and A. Roorda, "MEMS based Adaptive Optics Scanning Laser Ophthalmoscopy," *Opt. Lett.* **31**, 1268-1270, 2006.
19. Y. Zhang and A. Roorda, "MEMS deformable mirror for ophthalmic imaging," *MEMS/MOEMS Components and Their Applications III*, edited by Scot S. Olivier, Srinivas A. Tadigadapa, Albert K. Henning, *Proc. of SPIE Vol. 6113*, 61130A, 2006.
20. Y. Zhang and A. Roorda, "Adaptive optics scanning laser ophthalmoscope using a micro-electro-mechanical (MEMS) deformable mirror," *Ophthalmic Technologies XVI*, edited by Fabrice Manns, Per G. Soderberg, Arthur Ho, *Proc. of SPIE Vol. 6138*, 61380Z, 2006.
21. S. Poonja, S. Patel, L. Henry, A. Roorda. "Dynamic visual stimulus presentation in an adaptive optics scanning laser ophthalmoscope", *Journal of Refractive Surgery*, **21**, 575-580, 2005.
22. American National Standard on the Safe use of Lasers, ANSI Z136.1-2000, American National Standards Institute, 2000.
23. T. G. Bifano, J. A. Perreault, P. A. Bierden, and C. E Dimas, "Micromachined deformable mirrors for adaptive optics," *High Resolution Wavefront Control: Methods, Devices, and Applications IV*, J. D. Gonglewski, M. A. Vorontsov, M. T. Gruneisen, S. R. Restaino, and R. K. Tyson, eds. *Proc. of SPIE Vol. 4825*, 10-13, 2002.
24. N. Doble, G. Yoon, P. Bierden, L. Chen, S. Olivier, and D. R. Williams, "Use of a microelectromechanical mirror for adaptive optics in the human eye", *Opt. Lett.*, **27**, 1537-1539. 2002.
25. N. Doble and D. R. Williams, "The application of MEMS technology for adaptive optics in vision science", *IEEE Journal of Selected Topics in Quantum Electronics*, **10**, 629-635, 2004.
26. N. Doble, M. T. Miller, G. Yoon, M. A. Helbrecht and D. R. Williams, "Wavefront corrector requirements for compensation of ocular aberrations in two large populations of normal human eyes," *Ophthalmic Technologies XVI*, edited by Fabrice Manns, Per G. Soderberg, Arthur Ho, *Proc. of SPIE Vol. 6138*, 61380X, 2006.
27. J. Porter, A. Guirao, I. G. Cox, and D. R. Williams, "Monochromatic aberrations of the human eye in a large population", *J. Opt. Soc. Am. A*, **18**, 1793-1803, 2001.

28. L. N. Thibos, X. Hong, A. Bradley, and X. Cheng, "Statistical variation of aberration structure and image quality in a normal population of healthy eyes", *J. Opt. Soc. Am. A*, **19**, 2329-2348, 2002.
29. A. Roorda and Y. Zhang. "Mechanism for cone reflectance revealed with low coherence AOSLO imaging," *Invest. Ophthalmol. Vis. Sci.* **46**, E-Abstract 2433. 2005.
30. Y. Zhang and A. Roorda, "New Generation Clinically Deployable Adaptive Optics Scanning Laser Ophthalmoscope," *Invest. Ophthalmol. Vis. Sci.* **47**, E-Abstract 1810. 2006.
31. T. Wilson, "The role of the pinhole in confocal imaging systems," Chap. 11 in *The Handbook of Biological Confocal Microscopy*, 2nd Edition, J. B. Pawley, Eds., pp. 167–182, Plenum, New York, 1995.
32. C. R. Vogel, D. Arathorn, A. Roorda, and A. Parker, "Retinal motion estimation and image dewarping in adaptive optics scanning laser ophthalmoscopy", *Opt. Express*, **14**, 487-493, 2006.
33. J. L. Duncan, Y. Zhang and A. Roorda, "Adaptive optics imaging of macular photoreceptors reveals differences in patients with retinitis pigmentosa and Cone-Rod Dystrophy." *Invest. Ophthalmol. Vis. Sci.* **47**, E-Abstract 5667/B761. 2006.